AIMS Mathematics

http://www.aimspress.com/journal/Math

AIMS Mathematics, 11(6): 18917–18942.
DOI: 10.3934/math.2026770
Received: 11 February 2026
Revised: 14 June 2026
Accepted: 18 June 2026
Published: 26 June 2026

Research article

Phase portraits, detection of chaos, and solitary wave solutions of the first extended (3+1)-dimensional KP equation for nonlinear optical systems

Ejaz Hussain[1], Nida Raees[2], Ali. H. Tedjani[3], Yakup Yildirim[4,5] and Taha Radwan[6,*]

[1] Institute of Mathematics, University of the Punjab, Quaid-e-Azam Campus, Lahore 54590, Pakistan
[2] Centre for High Energy Physics, University of the Punjab, Quaid-e-Azam Campus, Lahore 54590, Pakistan
[3] Department of Mathematics and Statistics, College of Science, Imam Mohammad Ibn Saud Islamic University (IMSIU), Riyadh 11564, Saudi Arabia
[4] Department of Computer Engineering, Biruni University, Istanbul 34010, Turkey
[5] Mathematics Research Center, Near East University, 99138 Nicosia, Cyprus
[6] Department of Management Information Systems, College of Business and Economics, Qassim University, Buraydah 51452, Saudi Arabia

* **Correspondence:** Email: t.radwan@qu.edu.sa.

Abstract: This investigation gives a comprehensive dynamical and analytical analysis of the first extended (3+1)-dimensional Kadomtsev-Petviashvili (eKP) equation, which is featured in the fields of non-linear optics and wave propagation. By the method of traveling wave transformation, the nonlinear partial differential equation is transformed into a planar dynamical system, and detailed phase plane and bifurcation analysis can be done. We analyze the qualitative characteristics of equilibrium points, i.e., centers, saddles, and cusps, for different physical conditions. An external periodic disturbance is introduced to study some complicated dynamics, and we observe chaos using a number of diagnostic tools, such as phase portraits, time series, return maps, Lyapunov exponents, and multistability analysis. A sensitivity study indicates that the dynamics of the waves depend greatly upon the initial condition, and this reveals the non-linear, unpredictable nature of the system. In parallel with the dynamical study, we obtained exact analytical solutions to the eKP equation with the help of a bilinear form. We applied various newly developed analytical techniques to obtain exact solutions, such as homoclinic solutions, multiwave solutions, and M-type rational solutions. We obtained homoclinic breather waves, M-type and rational waves, and multi-wave interactions, which exhibit localized oscillating states, stable rogue-wave solutions, and wave-number coupling. Plots show the robustness and toughness of these solutions. Merging dynamic insights and precise solutions of the extended KP model allows a better understanding of the complex nonlinear behavior, opening new horizons in soliton theory as well as applications in the fields of nonlinear optics, fluid mechanics, and complex wave systems.

Keywords: mathematical modeling; extended (3+1)-dimensional Kadomtsev-Petviashvili (eKP) equation; bifurcation analysis; chaotic structure; multi-stability analysis; return map; sensitivity analysis
Mathematics Subject Classification: 26A48, 26A51, 33B10, 37K40, 39B62

1. Introduction

Nonlinear evolution equations (NLEEs) are fundamental equations in the mathematical and physical fields of nonlinearity. They are an accurate representation of the dynamic behavior of complex systems over time and form the basis of basic research, representing realistic representations of many real-world phenomena. The major task is to obtain accurate solutions that give more insight into the theory and enhance the precision of practical prediction. A very important concept in this fight is integrability, which is a criterion for assessing whether an equation can be solved exactly. The concept of integrability may not be clear in all cases, since, depending on which analytical or algebraic point of view one chooses, an equation may be integrable or not. Various analytical tools have been derived to determine integrability of, e.g., Painlevé analysis [1], inverse scattering transform [2], Hirota's bilinear method [3], Lie symmetry analysis [4], bilinear neural network method [5], infinite conservation laws [6], Darboux transformations [7], Lax pairs [8], bilinear residual neural network method [9], and Bäcklund transformations [10]. Each of these approaches has provided important information about the basic structure and solvability of NLEEs [11–13].

Over the last few years, many analytical and numerical methods have appeared to investigate the complex behavior of nonlinear evolution equations. For example, the Kudryashov technique is used to generate exact traveling wave solutions for the space-time fractional coupled equal width wave equation (CEWE) and the space-time fractional coupled modified equal width wave equation (CMEWE) [14]. Furthermore, reaction-diffusion systems, including the Fitzhugh-Nagumo equation, have been studied extensively for multistability and bifurcation phenomena, which have provided a profound understanding of the interaction of coexisting attractors and their sensitivity to initial conditions [15]. The electroosmotic effect on micropolar pulsatile bloodstream through aneurysms and stenoses has been demonstrated to cause significant nonlinear wave modifications in the context of wave propagation in complex media [16]. Further, an advanced analytical technique has been employed to approach the fractional perturbed nonlinear Schrödinger equation and find optical soliton solutions, and this is another demonstration of the broad applicability of the nonlinear wave theory [17]. As a whole, these pieces highlight the importance of the current research and place it in a dynamic and growing research field.

Bifurcation analysis explains how it is possible to use a powerful mathematical approach for understanding how small changes in system features can bring about sudden and large changes in the behavior of dynamical systems. It identifies critical points in which a system changes from one state to another, and allows the prediction and control of complex dynamics in various areas of science and technology. In the field of engineering, bifurcation analysis is one of the ways to anticipate and prevent structural failures [18]. More specifically, in fluid dynamics, it makes sense in the phenomenon of the transition from laminar flow to turbulent flow [19]. In terms of biology, it exposes the interconnection between minor changes in conditions affecting population dynamics and disease transmission [20]. Bifurcation analysis can be especially related to chaos theory, which deals with the complexity and nonlinearity of the workings of nonlinear dynamic systems that become unpredictable. By discovering the workings of bifurcation, researchers will be able to map out which routes lead to chaos and to predict the behavior of chaos in both natural and manmade settings. This is an important relationship in the fields of meteorological forecasting, ecological modeling, and financial markets analysis [21, 22]. Studying chaotic events helps in understanding how highly sensitive systems with simple rules can generate complex and unpredictable patterns, even though those systems are controlled by very simple rules. But, examining how small changes in parameters or initial conditions can result in dramatically different outcomes allows us to gain a better understanding of the stability, resilience, and predictability of systems to help stakeholders make more informed decisions by improving the ability to model networks of interacting systems [23, 24]. The standard integrable Kadomtsev-Petviashvili (KP) equation is stated as follows [25, 26]:

$$(Q_{\mathcal{T}} + 6QQ_{\mathcal{X}} + Q_{\mathcal{XXX}})_{\mathcal{X}} + a_1 Q_{\mathcal{YY}} = 0, \tag{1.1}$$

which admits the weakly dispersive waves, with a quadratic nonlinear term $(QQ_{\mathcal{X}})_{\mathcal{X}}$, and a weak dispersion term $Q_{\mathcal{XXXX}}$. Equation (1.1) characterizes the phenomenon of small surface tension in comparison to the gravitational force in fluid dynamics, and appears in many physical settings [27,28]. The equation reads as

$$Q_{\mathcal{TT}} - Q_{\mathcal{XXXX}} - Q_{\mathcal{XX}} - 3(Q^2)_{\mathcal{XX}} = 0, \tag{1.2}$$

where $Q = Q(\mathcal{X}, \mathcal{T})$ is a real-valued, sufficiently often differentiable function that represents the height of the free surface of a fluid, and the subscript represents the partial derivative. The Boussinesq equation (1.2) models small-amplitude dispersive waves in shallow water propagating in both right and left directions [28–30]. Moreover, an extended KP was proposed as [25, 26, 31]:

$$(Q_{\mathcal{T}} + 6QQ_{\mathcal{X}} + Q_{\mathcal{XXX}})_{\mathcal{X}} - Q_{\mathcal{YY}} + \beta Q_{\mathcal{TT}} + \alpha Q_{\mathcal{TY}} = 0, \tag{1.3}$$

where $\beta Q_{\mathcal{TT}}$ and $\alpha Q_{\mathcal{TY}}$ are added to the standard KP equation (1.1), $Q = Q(\mathcal{X}, \mathcal{Y}, \mathcal{T})$ is a differentiable function, and β and α are nonzero constants.

This work is the first study of Eq (1.4), which has not been solved previously, using the localized wave behavior by homoclinic breather waves, M-type and rational waves, and multi-wave interactions. The study also provides a comprehensive dynamical analysis that includes phase-portrait studies and the detection of chaos using different tools such as 2D phase-portrait analysis, time-series analysis, return map, bifurcation diagram, multi-stability, sensitivity analysis on different initial conditions, and the Lyapunov exponent. The first extended (3+1)-dimensional KP (eKP) can be considered as follows [32]:

$$(Q_{\mathcal{T}} + 6QQ_{\mathcal{X}} + Q_{\mathcal{XXX}})_{\mathcal{X}} + a_1 Q_{\mathcal{XX}} + a_2 Q_{\mathcal{XY}} + a_3 Q_{\mathcal{XZ}} + a_4 Q_{\mathcal{YY}} = 0, \tag{1.4}$$

where $Q = Q(\mathcal{X}, \mathcal{Y}, \mathcal{Z})$ is a differential function with respect to the spatial variables $\mathcal{X}$, $\mathcal{Y}$, and $\mathcal{Z}$, the temporal variable $\mathcal{T}$, and a_i, $i = 1, 2, 3, 4$, are nonzero arbitrary parameters. The additional terms in Eq (1.4), $a_1 Q_{XX}, a_2 Q_{XY}, a_3 Q_{XZ}, a_4 Q_{YY}$, represent different physical mechanisms of wave evolution: Q_{XX}: longitudinal dispersion correction; Q_{XY} and Q_{XZ}: cross-directional coupling effects, modeling interaction between different spatial directions; Q_{YY}: transverse dispersion along another spatial axis. Equation (1.4) is introduced to extend the KP framework to (3+1)-dimensions, enabling modeling of multi-directional wave propagation and spatial coupling effects. The added terms represent anisotropic dispersion and cross-interactions between spatial directions, which are essential in physical systems such as nonlinear optics and plasma. This extension provides a more realistic and comprehensive description of complex wave dynamics and allows the discovery of new nonlinear phenomena. Abdul Majid Wazwaz investigated the initial extended (3+1)-dimensional KP equation by Painlevé analysis, deriving lump solutions and multi-soliton solutions [32]. Many other studies about the KP equation have been discussed here [33–35].

The following is the organization of the paper. In Section 2, we formulate the transformation of the partial differential equation (PDE) into an ordinary differential equation (ODE) by using the traveling wave transformation. Section 3 presents the dynamical-system analysis, in which the phase portraits are analyzed for the quantitative evaluation of the influence of the system parameters, and the chaos is detected by the two-dimensional phase portraits, time series analysis, and multistability analysis. Section 4 is focused on sensitivity analysis. An analytical study in Section 5 is performed, including the derivation of the bilinear form and the construction of breather, rational, and multi-wave solutions. Section 6 discusses the results and discussion, and Section 7 shows the future work. Finally, Section 8 provides a detailed discussion as well as conclusions.

2. Mathematical formulations of the governing model

This part provides the mathematical analysis of the examined model. We concentrate on analyzing its fundamental properties using both analytical and numerical methods. We consider a general nonlinear partial differential equation of the form

$$M(Q, Q_{\mathcal{T}}, Q_{\mathcal{X}}, Q_{\mathcal{Y}}, Q_{\mathcal{Z}}, Q_{\mathcal{XY}}, Q_{\mathcal{XZ}}, Q_{\mathcal{YZ}}, Q_{\mathcal{TT}}, Q_{\mathcal{XX}}, \dots) = 0, \tag{2.1}$$

where $Q = Q(\mathcal{X}, \mathcal{Y}, \mathcal{Z}, \mathcal{T})$ is a sufficiently smooth function. Using the following traveling wave transformation, we can convert the nonlinear partial differential equations (NLPDEs) into nonlinear ordinary differential equations (NLODEs):

$$Q(\mathcal{X}, \mathcal{Y}, \mathcal{Z}, \mathcal{T}) = \Delta(\rho), \quad \rho = \mathcal{X} + K\mathcal{Y} + V\mathcal{Z} - \Theta\mathcal{T}, \tag{2.2}$$

where K and V are arbitrary constants and Θ indicates the speed of wave. By substituting Eq (2.2) into Eq (2.1), as a consequence, we get the following NLODE:

$$M(\Delta, \Delta_\rho, \Delta_{\rho\rho}, \Delta_{\rho\rho\rho}, \dots) = 0. \tag{2.3}$$

Governing model

In particular, the eKP equation is given by

$$(Q_{\mathcal{T}} + 6QQ_{\mathcal{X}} + Q_{\mathcal{XXX}})_{\mathcal{X}} + a_1 Q_{\mathcal{XX}} + a_2 Q_{\mathcal{XY}} + a_3 Q_{\mathcal{XZ}} + a_4 Q_{\mathcal{YY}} = 0. \tag{2.4}$$

By plugging Eq (2.2) into Eq (2.4), we obtain the following result:

$$(a_4K^2 + a_2K + a_3V - \Theta + 6\Delta + a_1)\Delta_{\rho\rho} + 6\Delta_\rho^2 + \Delta_{\rho\rho\rho\rho} = 0. \tag{2.5}$$

Integrating twice, Eq (2.5) becomes

$$\Delta_{\rho\rho} + 3\Delta^2 + (a_4K^2 + a_2K + a_3V - \Theta + a_1)\Delta = 0. \tag{2.6}$$

The reduction from Eq (2.5) to Eq (2.6) is obtained by integrating twice with respect to ρ. This procedure introduces integration constants. However, for solitary wave solutions with decaying boundary conditions $\Delta, \Delta_\rho \to 0$ as $|\rho| \to \pm\infty$, all integration constants vanish. Therefore, the resulting reduced equation is written in the simplified form given in Eq (2.6) without loss of generality.

3. Dynamical analysis

This section illustrates the dynamical investigation of the proposed model adopting several techniques, such as bifurcation analysis, sensitivity assessment, and chaos detection. A wide range of qualitative instruments is utilized, including 2D phase portrait, time series analysis, multistability, return map, bifurcation diagram, and sensitivity structure.

3.1. Phase portrait analysis

Bifurcation analysis is a crucial mathematical tool for examining changes in the qualitative behavior of a dynamical system as its parameters vary. In nonlinear evolution equations, small alterations in physical parameters can result in substantial modifications to the structure and stability of equilibrium points. These changes are termed bifurcations. Analyzing the equilibrium points and their stability using the Jacobian matrix allows for the determination of whether the system displays center, saddle, or cusp behavior. These alterations offer significant understanding of the fundamental wave dynamics and assist in discerning the conditions that may lead to stable periodic motions, separatrix structures, or unstable trajectories. Bifurcation analysis within the current model elucidates how parameter differences affect the qualitative qualities of phase portraits and, subsequently, the propagation properties of nonlinear waves governed by the extended KP equation. We examine the phase portrait analysis of the model utilizing the Galilean transformation on Eq (2.6), resulting in the unperturbed traveling wave system [36, 37].

$$\begin{cases} \dfrac{d\Delta}{d\rho} = M, \qquad \dfrac{dM}{d\rho} = -3\Delta^2 - P\Delta, \\ P = (a_4K^2 + a_2K + a_3V - \Theta + a_1). \end{cases} \tag{3.1}$$

It describes a dynamical system with the Hamiltonian function established as

$$H^\star(\Delta, M) = \frac{M^2}{2} + \Delta^3 + \frac{P\Delta^2}{2} = h. \tag{3.2}$$

It is worth noting that the Hamiltonian structure in Eq (3.2) is derived from the traveling-wave reduction of the governing nonlinear evolution equation through the Galilean transformation. Unlike classical Hamiltonian systems, where the potential energy is prescribed a priori, the present Hamiltonian is reconstructed directly from the reduced dynamical system using the relation

$$\frac{dM}{d\rho} = -\frac{\partial H^\star}{\partial \Delta}.$$

In this formulation, the Hamiltonian represents an energy-like invariant of the system rather than a mechanical energy function. The cubic term Δ^3 arises naturally from the nonlinear self-interaction terms of the original extended KP equation after reduction. Therefore, the Hamiltonian structure is fully consistent with the nonlinear and integrable nature of the model, where h is referred to as the Hamiltonian constant. Hamiltonian function states that it is the sum of kinetic energy and potential energy. In Eq (3.2), $\frac{M^2}{2}$ is the kinetic energy and $\Delta^3 + \frac{P\Delta^2}{2}$ is potential energy. Now we find the equilibrium points of the dynamical system described in Eq (3.1).

$$\begin{cases} M = 0, \\ -3\Delta^2 - P\Delta = 0. \end{cases} \tag{3.3}$$

To solve the system (3.3), we get the following equilibrium points:

$$\mathcal{A} = (0,0), \quad \mathbf{B} = \left(\frac{-P}{3}, 0\right). \tag{3.4}$$

In addition, the Jacobian matrix of Eq (3.1) is given by

$$J^{\star}(\Delta, M) = \begin{vmatrix} 0 & 1 \\ -6\Delta - P & 0 \end{vmatrix},$$

$$J^{\star}(\Delta, M) = 6\Delta + P. \tag{3.5}$$

Remark: When analyzing a dynamical system, we can observe the behavior of points:

- If$J^{\star}(\mathcal{A}, \mathcal{B}) > 0$, then point is a center.
- If $J^{\star}(\mathcal{A}, \mathcal{B}) < 0$, then point is a saddle.
- If $J^{\star}(\mathcal{A}, \mathcal{B}) = 0$, then point is a cusp.

Different cases are discussed on the dynamical system (3.1) depending on the parameter in Tables 1 and 2.

Table 1. Bifurcation analysis for Figure 1.

Figure	Parameters case	Parameter values	Behavior of points
1(a)	$P > 0$	$\Theta = 1.1$, $a_4 = 1$, $a_3 = 1$, $a_2 = 1.2$, $a_1 = 0.2$, $V = 0.9$, $K = 2.5$	$J^{\star}(A) > 0$, $J^{\star}(B) < 0$
1(b)	$P < 0$	$\Theta = 1.1$, $a_4 = -1$, $a_3 = 1$, $a_2 = 1.2$, $a_1 = 0.2$, $V = 0.9$, $K = 2.5$	$J^{\star}(A) < 0$, $J^{\star}(B) > 0$

Table 2. Classification of phase portraits based on parameter conditions.

Plot	Cases	Points	ICs
1(a)	$P > 0$	(0,0), (-2.04,0)	(-0.2, 0.02), (-0.4, 0.02), (-0.6, 0.02), (-0.8, 0.02), (-1, 0.02), (-1.2, 0.02), (-1.4, 0.02), (-1.8, 0.02), (-2, 0.4), (-2, 0.8), (-2, 1), (-2,1.2), (-2.1, 0.02), (-2.3, 0.02), (-2.4, 0.02), (-2.5, 0.02), (-2.6, 0.02), (-2.7, 0.02)
1(b)	$P < 0$	(1.09,0), (0,0)	(1.1, 0.5), (1.3, 0.5), (1.4, 0.5), (1.5, 0.5), (1.55, 0.5), (1.6, 0.5), (1.62, 0.5), (1.63, 0.5), (1.65, 0.5), (1.67, 0.5), (1.68, 0.5), (-0.2, 0.2), (-0.3, 0.2), (-0.4, 0.2), (-0.5, 0.2), (-0.6, 0.2)

Results: As a consequence, it can be easily demonstrated from Figure 1(a) that there are two points, the first one is $\mathcal{A}$ and the second is $\mathcal{B}$. The first point $\mathcal{A}$ represents the center of the dynamical system that is described in Eq (3.1), and the second point $\mathcal{B}$ shows the behavior of saddle points.

Conversely, in Figure 1(b), the point $\mathcal{A}$ shows the saddle point and $\mathcal{B}$ represents the center point of the dynamical system (3.1).

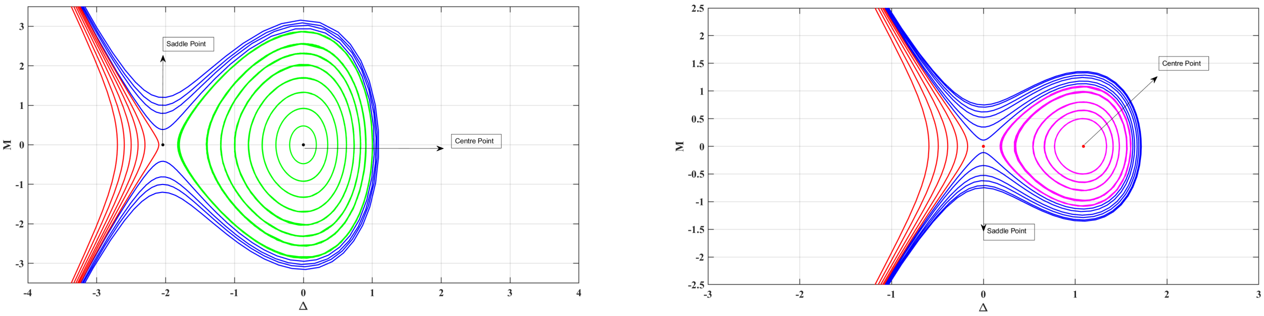

(a) $P > 0$ **(b)** $P < 0$

Figure 1. Analysis of phase trajectories in two-dimensional plots for the unperturbed system (3.1) under different parametric effects (a) $P > 0$, and (b) $P < 0$.

3.2. *Chaotic analysis*

Chaotic dynamics are defined by a pronounced sensitivity to initial conditions, indicating that small variations in the system's initial state can result in vastly divergent long-term behaviors. This study employs many diagnostic tools to detect and analyze chaotic dynamics, including two-dimensional phase portraits, time-series analysis, and multistability investigations. Phase portraits facilitate the depiction of trajectories inside the phase space of a dynamical system, where chaotic attractors express complex and non-periodic formations. Time-series plots indicate non-repetitive irregular oscillations, whereas multistability analysis illustrates the presence of several dynamical states, including periodic, quasi-periodic, and chaotic motions, contingent upon beginning conditions. These results offer compelling evidence of deterministic chaos in the disturbed system and underscore the intricate nonlinear dynamics of the extended KP model. Comprehending chaotic structures is crucial for analyzing nonlinear wave interactions and forecasting the stability and development of wave patterns in physical systems, including nonlinear optical media, fluid dynamics, and plasma settings. In this section, we study the perturbed system by adding the perturbation term $\delta\cos(\mu\rho)$ in the dynamical system (3.1), leading to the modified system [38, 39] given below:

$$\begin{cases} \dfrac{d\Delta}{d\rho} = M, \qquad \dfrac{dM}{d\rho} = -3\Delta^2 - P\Delta + f(\rho), \end{cases} \tag{3.6}$$

where $P = (a_4K^2 + a_2K + a_3V - \Theta + a_1)$ and $f(\rho) = \delta\cos(\mu\rho)$. The term $\delta\cos(\mu\rho)$ is referred to as the perturbation, where δ denotes the amplitude and μ represents the frequency of the external forcing applied to the system described by Eq (3.6). This external perturbation can induce periodic, quasi-periodic, or chaotic wave structures. The investigation keeps all other physical parameters of the system in (3.6) constant. In our research, we found that system (3.6) shows chaotic behavior, meaning its motion is unpredictable and does not follow a regular pattern over time. To identify this chaos, we used several methods, including 2D phase portraits, time series analysis, and multistability.

3.2.1. Phase portrait and time analysis

Using 2D phase portraits and time series analysis, we are able to detect the presence of chaos. Strange attractors display trajectories that are very sensitive and non-repetitive. The hallmark of chaos is the extreme sensitivity to the initial conditions of a system, as demonstrated by irregular aperiodic swings in a time series. In order to investigate the perturbed system, we plotted the time evolution of the Lyapunov exponents and different phase pictures. We solved the system using the fourth-order Runge-Kutta (RK4) scheme applied to Eq (3.6). Our results indicate that Eq (3.6) behaves chaotically for both positive and negative values of the parameter P, as shown in Figures 2–5 with many different initial conditions and parameter values $P = 2$, $\delta = 0.5$, $\mu = 0.6$.

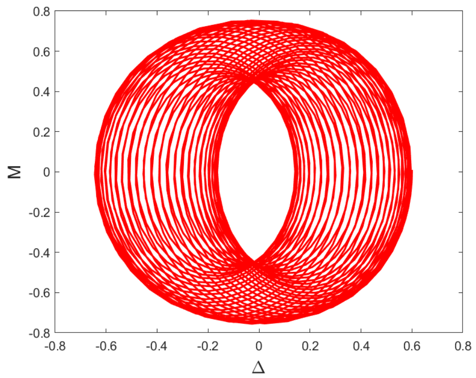

(a) 2D phase portraits

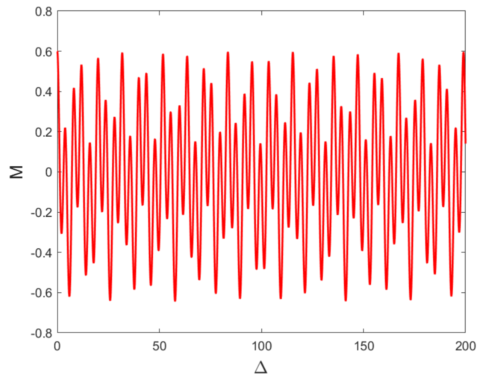

(b) Time series analysis

Figure 2. 2D phase portraits and time series analysis by using different initial conditions $(0.6, 0.01)$ causes the dynamical system (3.6) to exhibit chaotic behavior with suitable parametric values $P = 2$, $\delta = 0.5$, and $\mu = 0.6$.

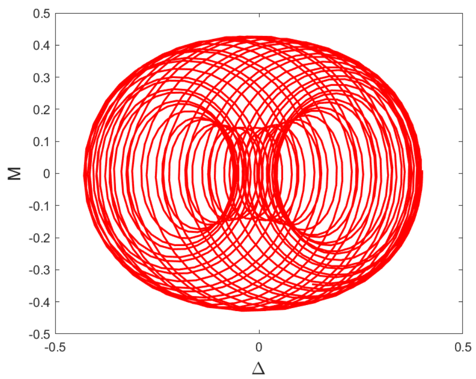

(a) 2D phase portraits

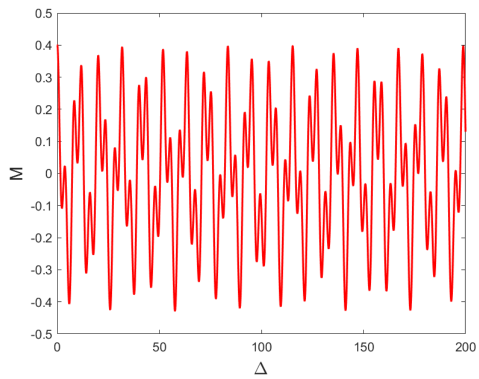

(b) Time series analysis

Figure 3. 2D phase portrait and time series analysis of the dynamical system (3.6), by employing different initial conditions $(0.4, 0.01)$, and parameter values $P = 2$, $\delta = 0.5$, and $\mu = 0.6$.

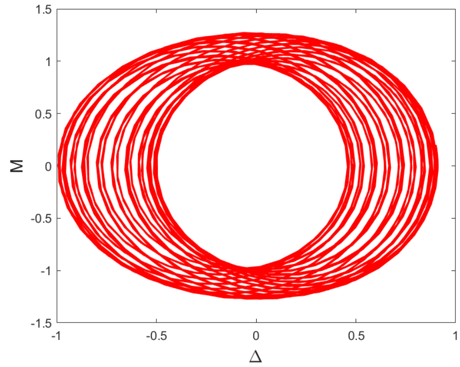

(a) 2D phase portraits

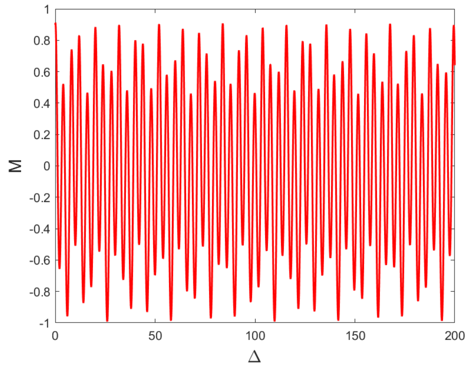

(b) Time series analysis.

Figure 4. The chaotic behavior of the dynamical system (3.6), which is characterized by the various initial conditions $(0.9, 0.2)$ with suitable parameter values.

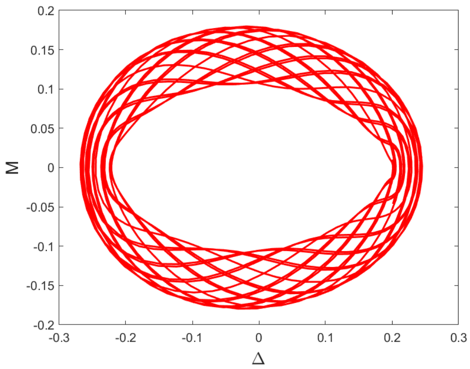

(a) 2D phase portraits

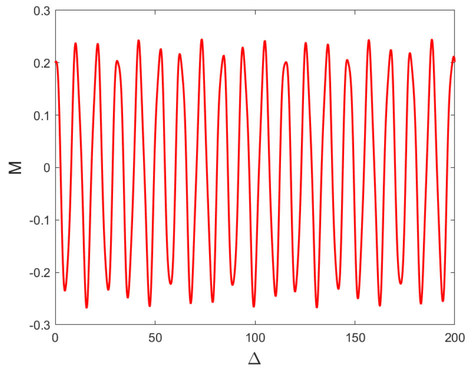

(b) Time series analysis

Figure 5. Chaotic behavior of the dynamical system (3.6) using the 2D phase portrait and time series analysis with various initial conditions $(0.2, 0.01)$.

3.2.2. Multistability analysis

In this section, we provide further analysis to investigate the possibility of multistability in the system (3.6). The system can display several dynamic behaviors depending on the initial conditions. These behaviors include chaotic behavior, quasi-periodic behavior, and periodic behavior, which appear under certain circumstances. Multistability of the perturbed system (3.6) is shown for the parameter set ($P = 2$, $\delta = 0.5$, $\mu = 0.6$). In Figure 6(a), a periodic orbit is obtained for the initial condition $(0.9, 0.2)$ (red curve), while a chaotic orbit appears for $(0.9, 0.1)$ (blue curve). In Figure 6(b), periodic behavior is observed for the initial condition $(0.2, 0.01)$ (red curve), whereas chaotic behavior occurs for $(0.2, 0.3)$ (blue curve). The coexistence of periodic and chaotic attractors with the same system parameters but different initial conditions confirms multistability.

In Figure 7(a), a periodic orbit is obtained for the initial condition $(0.9, 0.5)$ (red curve), while a chaotic orbit appears for $(0.9, 0.4)$ (blue curve). In Figure 7(b), periodic behavior is observed for $(0.4, 0.01)$ (red curve), whereas chaotic behavior occurs for $(0.4, 0.001)$ (blue curve). The coexistence of periodic and chaotic attractors for identical parameters but different initial conditions confirms multistability in system (3.6).

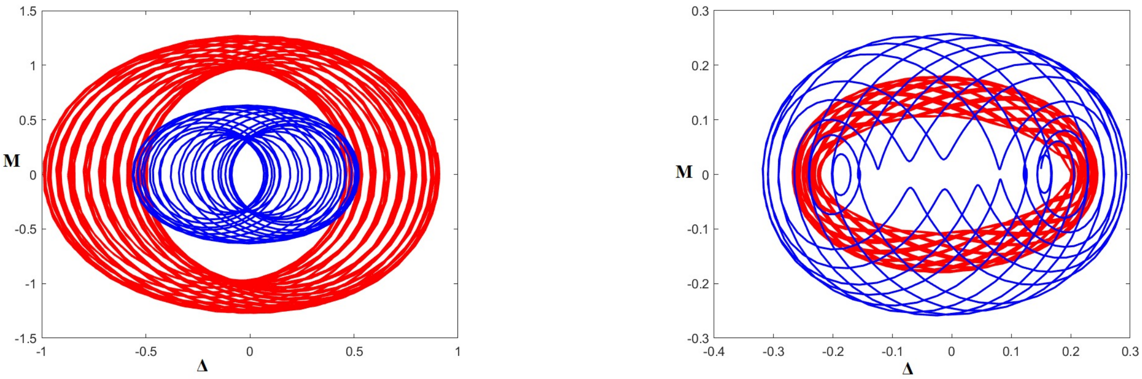

(a) (0.9, 0.2) and (0.9, 0.1) **(b)** (0.2, 0.01) and (0.2, 0.3)

Figure 6. Multistability of the perturbed system (3.6) for the parameter set (P = 2, δ = 0.5, μ = 0.6).

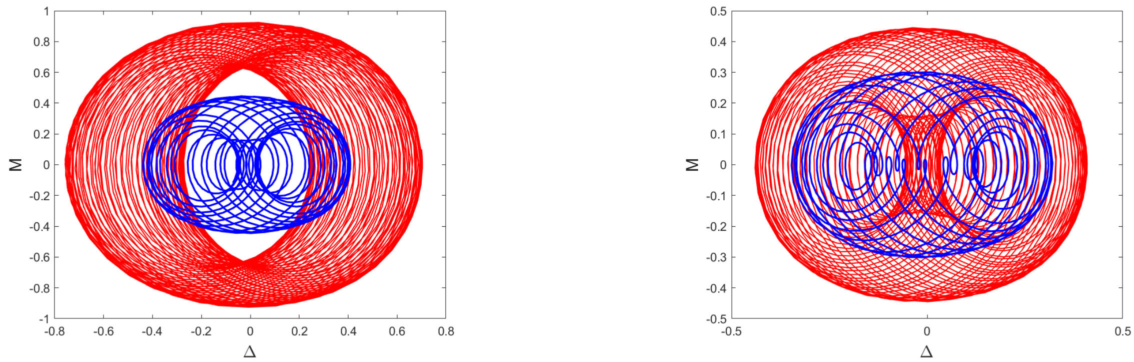

(a) (0.9, 0.5) and (0.9, 0.4) **(b)** (0.4, 0.01) and (0.4, 0.001)

Figure 7. Multistability of the perturbed system (3.6) is demonstrated for the parameter set (P = 2, δ = 0.5, μ = 0.6).

3.2.3. Lyapunov exponent

By examining the divergence or convergence of nearby trajectories, this method enables the evaluation of chaotic behavior using Lyapunov exponent values, as shown in Figure 8. It is important to note that Lyapunov exponents are just one of many techniques to detect chaos, providing a comprehensive analysis of the model's dynamics. A positive Lyapunov exponent indicates chaos, while a negative one suggests stability. Using this method, we identified chaos in the dynamical system (3.6) shown in Figure 8, resulting in two Lyapunov exponent values: $\lambda_1 = 0.0071$, $\lambda_2 = -0.0071$, and $\lambda_1 = 0.0298$, $\lambda_2 = -0.0298$ with other parameters values $p = 0.2$, $\delta = 0.1$, $\mu = 0.02$.

The Lyapunov exponents are calculated from the standard Wolf algorithm [40] with Gram-Schmidt orthonormalization, which is used to determine the rates at which nearby trajectories in the phase space diverge exponentially. The governing equation (3.6) is numerically integrated with the RK4 method with a constant step size $\Delta\rho = 0.1$. The total integration time is $T = 2000$, and the first $T_{trans} = 500$ time units are discarded as transient to ensure the computed exponents represent the asymptotic behavior. Convergence is checked by increasing the integration time and seeing if the values of the Lyapunov exponents converge to stable limits within 5 fluctuations. The result is a positive value for the largest Lyapunov exponent of the system $\lambda_1 \equiv 0.0071$ and a negative value for the second Lyapunov exponent of the system $\lambda_2 \equiv -0.0071$, clearly indicating the deterministic chaotic behavior of the system.

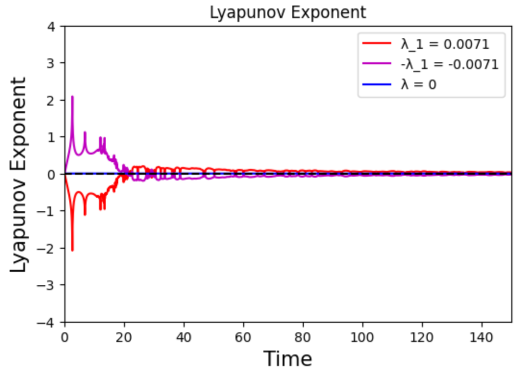

(a) $\mu = 0.25$ **(b)** $\mu = 0.05$

Figure 8. Representation of chaotic behavior through the Lyapunov exponent by using the suitable parametric values $\lambda_1 = 0.0071$, $\lambda_2 = -0.0071$, and $\lambda_1 = 0.0298$, $\lambda_2 = -0.0298$ with other parameter values $p = 0.2$, $\delta = 0.1$, $\mu = 0.02$.

3.2.4. Return map

The return map, which graphically represents successive points of a variable, elucidates the foundational patterns inherent within the system. Chaotic behavior is identified when the return map exhibits a dispersed, non-repetitive configuration as opposed to a smooth curve, thereby indicating a sensitive dependence on initial conditions. Figure 9 illustrates the detection of chaotic behavior in system (3.6) with parameters $a_4 = 1.5$, $a_2 = 2.2$, $a_3 = 2$, $a_1 = 0.2$, $K = 0.4$, $V = 3.8$, $P = 0.89$, $\Theta = 0.067$, $\delta = 2.3$, and $\mu = 0.01$.

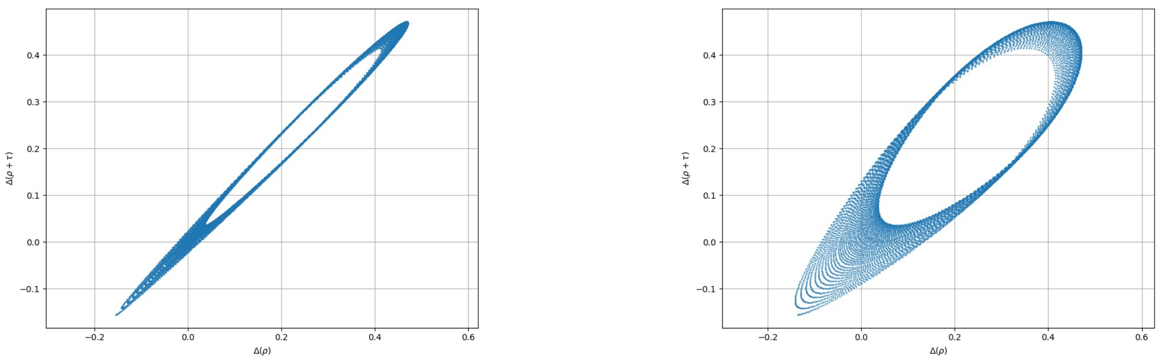

(a) $\tau = 0.042$ **(b)** $\tau = 0.19$

Figure 9. Representation of chaotic behavior through return map by using the suitable parametric values $a_4 = 1.5$, $a_2 = 2.2$, $a_3 = 2$, $a_1 = 0.2$, $K = 0.4$, $V = 3.8$, $P = 0.89$, $\Theta = 0.067$, $\delta = 2.3$, and $\mu = 0.01$ and initial condition $(0.1, 0.52)$.

3.3. Poincare mapp

Figure 10 presents the Poincaré maps of the perturbed dynamical system (3.6) for different initial conditions, providing strong evidence of deterministic chaos. In Figure 10(a), corresponding to the initial condition $(0.6, 0.01)$, the intersection points are irregularly scattered throughout the phase space rather than forming a finite set of discrete points or a smooth closed curve. This behavior indicates the presence of a strange attractor and confirms aperiodic chaotic motion. Figure 10(b), obtained for the initial condition $(0.4, 0.01)$, exhibits a similarly dispersed point distribution, although the attractor occupies a comparatively smaller region of the phase plane. The scattered nature of the points demonstrates that the trajectory does not repeat periodically and remains highly sensitive to perturbations. In Figure 10(c), corresponding to $(0.9, 0.2)$, the attractor becomes broader and more complex, covering a larger phase-space area. This wider distribution reflects stronger nonlinear interactions and enhanced chaotic oscillations, where trajectories continuously stretch and fold, a hallmark mechanism of deterministic chaos. Figure 10 (d), generated for the initial condition $(0.2, 0.01)$, also displays an irregular cloud of points without any discernible periodic structure, confirming the persistence of chaotic behavior. The irregular and scattered distribution of intersection points reveals the existence of strange attractors and confirms the presence of deterministic chaotic dynamics.

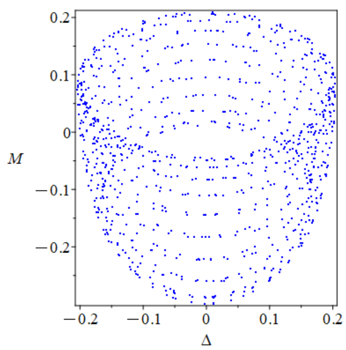

(a) Poincaré map for (0.6,0.01)

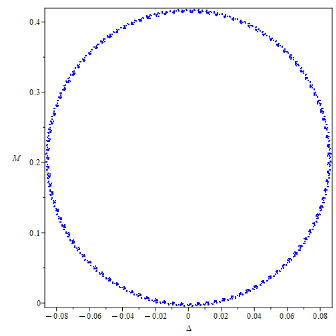

(b) Poincaré map for (0.4,0.01)

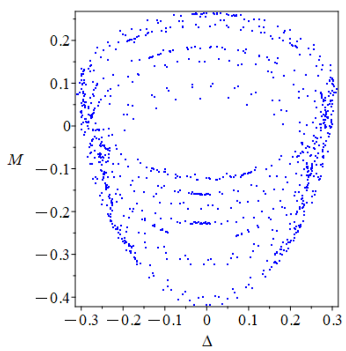

(c) Poincaré map for (0.9,0.2)

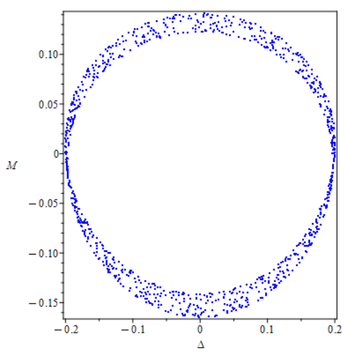

(d) Poincaré map for (0.2,0.01)

Figure 10. Poincaré maps of the perturbed dynamical system (3.6) for different initial conditions: (a) $(0.6, 0.01)$, (b) $(0.4, 0.01)$, (c) $(0.9, 0.2)$, and (d) $(0.2, 0.01)$, with parameter values $P = 2$, $\delta = 0.5$, and $\mu = 0.6$.

The concentration of points in certain regions indicates that the trajectory visits some states more frequently than others, which is characteristic of strange attractors. Overall, all four Poincaré maps reveal non-periodic and irregular structures, demonstrating that the perturbed extended KP system possesses chaotic dynamics and exhibits strong sensitivity to initial conditions. These findings indicate that even slight variations in the initial state can significantly alter the long-term evolution of nonlinear wave propagation, which is of considerable importance in applications involving nonlinear optics, plasma physics, and complex wave systems.

4. Sensitivity analysis

Sensitivity analysis is significant for interpreting how initial conditions affect the behavior of a nonlinear dynamical system. The trajectory of a system can be dramatically altered by a very small perturbation in the initial state in many nonlinear systems. This effect is usually known as sensitive dependence on initial conditions, which is among the most important properties of nonlinear and chaotic dynamical systems. We are interested in exploring this property in the proposed model by considering the unperturbed dynamical system below [41, 42]:

$$\begin{cases} \dfrac{d\Delta}{d\rho} = M, \\ \dfrac{dM}{d\rho} = -3\Delta^2 - (a_4K^2 + a_2K + a_3V - \Theta + a_1)\Delta. \end{cases} \tag{4.1}$$

All the system parameters remain constant in this analysis with the initial conditions slightly perturbed. The idea is to explore the effect of slight variation in the initial point on the further development of the wave. The RK4 method is used to carry out the numerical simulations in order to obtain stable and accurate computation of the trajectories.

Figures 11(a) and 12(b) demonstrate the system's sensitivity to differing initial conditions while maintaining constant parameters. The graphs exhibit periodic behavior, with the curves displaying sensitivity to initial conditions, resulting in amplitude fluctuations. Solitary waves are characterized by localized pulses and stable, non-dispersive wave packets. Sensitivity analysis has wide-ranging applications, including optimizing engineering designs, evaluating environmental impacts, and managing financial risks. In the medical field, it significantly contributes to drug development and understanding treatment variability, while in energy systems it enhances the efficiency of renewable energy sources. In Figure 11(a), there are two initial conditions (0.02,0) and (0.03,0) with different colors, red and green, respectively. In Figure 11(b), there are two initial conditions (0.04,0) and (0.02,0) with different colors, magenta and red, respectively. Similarly, in Figure 12(a), it can be easily shown by using two initial conditions and comparing the wave behavior (0.04,0) and (0.03,0) in magenta and green. Lastly, in Figure 12(b), three wave behaviors are shown with different conditions (0.02,0), (0.03,0), and (0.04,0) in red, green, and magenta. Sensitivity analysis establishes that the dynamical system proposed is highly sensitive to its initial conditions. The fact that the perturbations, even in the initial state, can drastically change the amplitude and development of the wave profiles testifies to the inherent nonlinear and complex nature of the extended KP model.

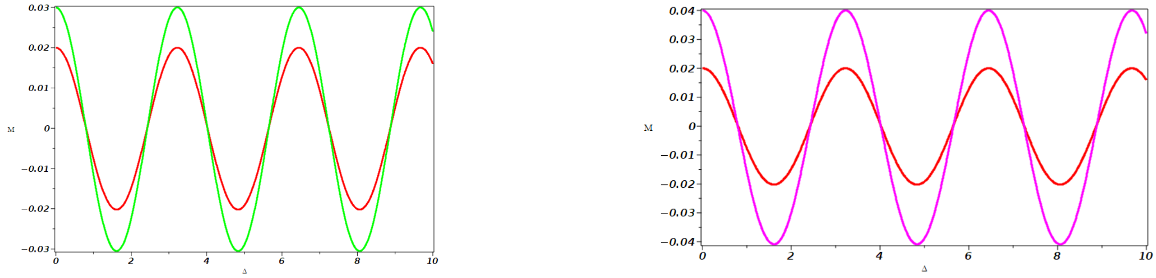

(a) Time series analysis with initial condition (0.02,0) **(b)** Time series analysis with initial condition (0.03,0)

Figure 11. Sensitivity analysis of the system (4.1) using the different initial conditions (0.02,0) and (0.03,0).

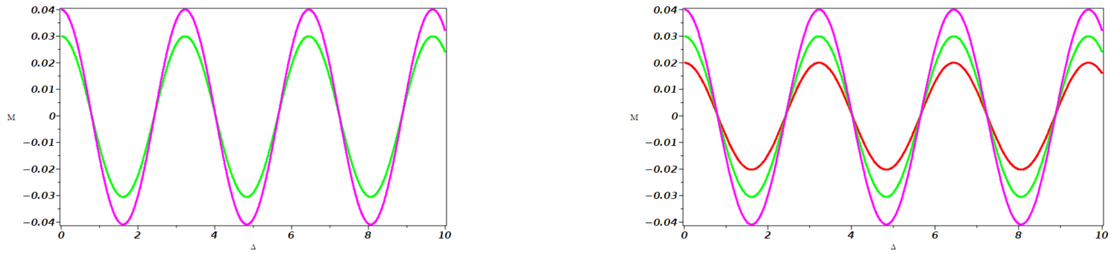

(a) Time series analysis with initial condition (0.04,0) **(b)** Time series analysis with initial condition (0.03,0)

Figure 12. Sensitivity analysis of the system (4.1) using the different initial conditions (0.04,0) and (0.03,0).

5. Breather, rational, and multi-wave solutions

This section presents the homoclinic breather, M-shaped rational, and multi-wave solutions for the first extended KP equation. These solutions illustrate the complex nonlinear wave dynamics of the model, encompassing localized oscillations, rogue-wave-type structures, and recurrent wave patterns.

5.1. Bilinear form

To investigate the nonlinear dynamics of the eKP equation, we reformulate it within the framework of the Hirota bilinear method [43]. The bilinear approach has been extensively applied in soliton theory, as it provides a systematic and elegant means of constructing various classes of exact solutions, including breather, rational, and multi-wave solutions. The crucial step in this procedure is the derivation of the associated bilinear form. To this end, we employ a logarithmic transformation, which transforms the original nonlinear equation into a bilinear representation that is more amenable to rigorous analysis and the systematic generation of exact solutions [44–46].

$$\Delta = 2\frac{d}{d\rho}\ln\left(f(\rho)\right) = 2\frac{f_\rho}{f}. \tag{5.1}$$

By differentiating with respect to ρ, higher-order derivatives such as Δ_ρ, $\Delta_{\rho\rho}$, and $\Delta_{\rho\rho\rho}$ are expressed in terms of f, f_ρ, $f_{\rho\rho}$, and $f_{\rho\rho\rho}$. Substituting these expressions into Eq (2.6) and simplifying by eliminating common factors of f, we obtain a polynomial equation in terms of f and its derivatives. Rearranging the resulting terms yields the bilinear form presented in the following expression:

$$\begin{aligned} & -2a_1 f^2 f_\rho + 2a_4 f^2 K^2 f_\rho + 2a_2 K f^2 f_\rho + 2a_3 f^2 V f_\rho - 2\Theta f^2 f_\rho \\ & + 4f_\rho^3 + 2f^2 f_{\rho\rho\rho} - 6f_{\rho\rho}(f f_\rho) + 12(f f_\rho)^2 = 0. \end{aligned} \tag{5.2}$$

For completeness, we recall the definition of Hirota's bilinear differential operators as

$$D_\rho^n(f \cdot f) = \left(\frac{\partial}{\partial \rho} - \frac{\partial}{\partial \rho'}\right)^n f(\rho)\, f(\rho')\Big|_{\rho'=\rho}. \tag{5.3}$$

In particular, the first and third-order Hirota operators are given by

$$D_\rho(f \cdot f) = 2 f f_\rho, \tag{5.4}$$

$$D_\rho^3(f \cdot f) = 2\left(f f_{\rho\rho\rho} - 3 f_\rho f_{\rho\rho} + 2 f_\rho^3\right). \tag{5.5}$$

Using these identities, we have the bilinear equation

$$\left(D_\rho^3 + (a_4 K^2 + a_2 K + a_3 V - \Theta + a_1) D_\rho\right) f \cdot f = 0, \tag{5.6}$$

which is exactly equivalent to Eq (5.2). Hence, the Hirota bilinear form and its expanded polynomial representation are fully consistent. The intermediate expressions in the following derivations may contain complex parameters or complex-valued functions f. The final wave field $\mathcal{Q}(\mathcal{X}, \mathcal{Y}, \mathcal{Z}, \mathcal{T}) = 2(\ln f)\rho$ is, however, guaranteed to be real under the imposed parameter conditions (e.g., if the sum of a complex function and its complex conjugate is used for f, or if the imaginary constants of the logarithmic derivative are set to zero). We confirm (explicitly) the reality of each solution type.

5.2. Homoclinic breather solution

In this section, we derive the breather solution by employing the following transformation [47]:

$$f = e^{-q\,(b_1\rho + b_2)} + r_1 e^{q\,(b_3\rho + b_4)} + r_2 \cos(q_1(b_5\rho + b_6)). \tag{5.7}$$

However, b_i $(1 \leq i \leq 6)$, r_1, r_2, q, q_1 are real coefficients to be determined. By substituting Eq (5.7) into Eq (5.2) and collecting the coefficients of $e^{-3q(b_2+b_1\rho)}$, $e^{-2q(b_2+b_1\rho)}$, $e^{-2q(b_2+b_1\rho)+q(b_4+b_3\rho)}$, $e^{-q(b_2+b_1\rho)+2q(b_4+b_3\rho)}$, $e^{2q(b_4+b_3\rho)}$, $e^{3q(b_4+b_3\rho)}$, $\sin^3(q_1(b_6+b_5\rho))$, $e^{q(b_4+b_3\rho)}\sin^2(q_1(b_6+b_5\rho))$, and $e^{-q(b_2+b_1\rho)}\sin^2(q_1(b_6+b_5\rho))$, we obtain a system of equations that determines the values of the parameters:

$$b_1 = b_1, \quad b_2 = b_2, \quad b_3 = -b_1, \quad b_4 = b_4, \quad b_5 = 0, a_1 = 0, \quad a_2 = \frac{-a_4 K^2 - a_3 V + \Theta}{K}. \tag{5.8}$$

Inserting Eq (5.8) into Eq (5.7), we have

$$f = e^{-q(b_2+b_1\rho)} + e^{q(b_4-b_1\rho)} r_1 + r_2 \cos(b_6 q_1). \tag{5.9}$$

Using Eq (5.9) in Eq (5.1), we get the following expression:

$$\Delta(\rho) = -\frac{2b_1 q\left(1 + e^{(b_2+b_4)q} r_1\right)}{1 + e^{(b_2+b_4)q} r_1 + e^{q(b_2+b_1\rho)} r_2 \cos(b_6 q_1)}. \tag{5.10}$$

By substituting Eq (5.10) into Eq (2.2), we obtain the homoclinic breather solution corresponding to Eq (1.1):

$$\mathcal{Q}(\mathcal{X},\mathcal{Y},\mathcal{Z},\mathcal{T}) = -\frac{2b_1 q\left(1+e^{(b_2+b_4)q}r_1\right)}{1+e^{(b_2+b_4)q}r_1+e^{q(b_2+b_1(X+KY+VZ-T\Theta))}r_2\cos(b_6 q_1)}. \tag{5.11}$$

It is important to note that the degree of localization in this solution depends strongly on parameter choices. For the selected parameter set, the solution exhibits predominantly periodic behavior with limited spatial localization.

5.3. M-shaped rational solution

In this section, we investigate M-shaped rational solutions characterized by a quadratic functional form. The M-shaped soliton is derived through the following transformation [48]:

$$f = (c_1\rho + c_2)^2 + (c_3\rho + c_4)^2 + c_5. \tag{5.12}$$

Here, the coefficients c_i $(1 \le i \le 5)$ are real. By substituting the expression of f from Eq (5.12) into Eq (5.2) and equating coefficients of like powers of ρ, we obtain a system of equations that determines the parameter values:

$$c_1 = c_1, \qquad c_2 = c_2, \qquad c_3 = c_3, \qquad c_4 = i\,c_2, \qquad c_5 = c_5, \tag{5.13}$$

If c_2, c_5, c_1, and c_3 are real constants, the parameter $c_4 = ic_2$ puts an imaginary unit in the expression for $f(\rho)$, but the resulting wave field $\Delta(\rho) = 2(\ln f)\rho$ is real. This is because $f(\rho)$ in (5.13) may be written as the sum of a complex function and its complex conjugate up to a real constant, so that $\ln f$ is real up to an imaginary additive constant that will vanish when differentiated. The physically relevant solution $\Delta(\rho)$ is obtained from (5.15), and it is evident that it is a real solution, as can be verified by direct substitution. The Hirota bilinear method for obtaining real rational solutions employs complicated intermediate forms, which is a common algebraic method. Inserting these parameter values into Eq (5.12), we get the following expression:

$$f = \rho^2 c_1^2 + 2\rho\, c_1 c_2 + 2i\rho\, c_2 c_3 + \rho^2 c_3^2 + c_5. \tag{5.14}$$

By substituting Eq (5.14) into Eq (5.1), we have the following form:

$$\Delta(\rho) = \frac{4\,(c_1 + ic_3)\,(\rho c_1 + c_2 - i\rho c_3)}{\rho^2 c_1^2 + 2\rho c_1 c_2 + 2i\rho c_2 c_3 + \rho^2 c_3^2 + c_5}. \tag{5.15}$$

Substituting Eq (5.15) into Eq (2.2) yields the M-shaped rational solution associated with Eq (1.1):

$$\begin{aligned}&\mathcal{Q}(X,Y,Z,T)\\ =&\frac{4(c_1+ic_3)\Big((X+KY+VZ-T\Theta)\,c_1+c_2-i(X+KY+VZ-T\Theta)\,c_3\Big)}{(X+KY+VZ-T\Theta)^2c_1^2+2(X+KY+VZ-T\Theta)c_1c_2+2i(X+KY+VZ-T\Theta)c_2c_3+(X+KY+VZ-T\Theta)^2c_3^2+c_5}.\end{aligned} \tag{5.16}$$

The expression in (5.16) is real-valued for all real values of the parameters c_1, c_2, c_3, and c_5.

5.4. Multi-wave solution

In this section, we derive the multi-wave solution, comprising both hyperbolic and trigonometric functions. For this purpose, we introduce the following transformations to construct the multi-wave framework [49]:

$$f = l_0 \cosh(d_1\rho + d_2) + l_1 \cos(d_3\rho + d_4) + l_2 \cosh(d_5\rho + d_6). \tag{5.17}$$

Here, l_i $(i = 0, 1, 2)$ and d_i $(1 \leq i \leq 6)$ are real parameters. By substituting the expression for f given in Eq (5.17) into Eq (5.2) and collecting the coefficients of $\cos(d_4 + d_3\rho)^2$, $\cos(d_4 + d_3\rho)\cosh(d_2 + d_1\rho)$, $\cosh(d_2 + d_1\rho)\cosh(d_6 + d_5\rho)$, $\cos(d_4 + d_3\rho)^2 \sin(d_4 + d_3\rho)$, $\cos(d_4 + d_3\rho)\cosh(d_2 + d_1\rho)\sin(d_4 + d_3\rho)$, $\cosh(d_2 + d_1\rho)^2 \sin(d_4 + d_3\rho)$, $\sinh(d_6 + d_5\rho)^3$, $\sinh(d_2 + d_1\rho)\sinh(d_6 + d_5\rho)^2$, and $\sinh(d_2 + d_1\rho)^2 \sinh(d_6 + d_5\rho)$, we obtain a system of equations that yields the following parameter values:

$$\begin{aligned} d_1 &= -\frac{\sqrt{-a_1 + a_2K + a_4K^2 + a_3V - \Theta}}{\sqrt{2}}, \qquad d_2 = d_2, \\ d_3 &= -\frac{\sqrt{a_1 - a_2K - a_4K^2 - a_3V + \Theta}}{\sqrt{2}}, \qquad d_4 = d_4, \;\; d_5 = 0. \end{aligned} \tag{5.18}$$

By substituting Eq (5.18) into Eq (5.17), we obtain the following expression:

$$\begin{aligned} f =& l_1 \cos\left(d_4 - \frac{\sqrt{a_1 - a_2K - a_4K^2 - a_3V + \Theta}}{\sqrt{2}}\rho\right) + l_2\cosh(d_6) \\ &+ l_0 \cosh\left(d_2 - \frac{\sqrt{-a_1 + a_2K + a_4K^2 + a_3V - \Theta}}{\sqrt{2}}\rho\right). \end{aligned} \tag{5.19}$$

By substituting the expression of f from Eq (5.19) into Eq (5.1), we obtain

$$\Delta(\rho) = \frac{N(\rho)}{D(\rho)}, \tag{5.20}$$

where

$$\begin{aligned} N(\rho) =& \sqrt{2}\Big(l_1\sqrt{a_1 - a_2K - a_4K^2 - a_3V + \Theta}\, \sin\Big(d_4 - \tfrac{\sqrt{a_1-a_2K-a_4K^2-a_3V+\Theta}}{\sqrt{2}}\rho\Big) \\ &- l_0\sqrt{-a_1 + a_2K + a_4K^2 + a_3V - \Theta}\, \sinh\Big(d_2 - \tfrac{\sqrt{-a_1+a_2K+a_4K^2+a_3V-\Theta}}{\sqrt{2}}\rho\Big)\Big), \\ D(\rho) =& l_1\cos\Big(d_4 - \tfrac{\sqrt{a_1-a_2K-a_4K^2-a_3V+\Theta}}{\sqrt{2}}\rho\Big) + l_2\cosh(d_6) + l_0\cosh\Big(d_2 - \tfrac{\sqrt{-a_1+a_2K+a_4K^2+a_3V-\Theta}}{\sqrt{2}}\rho\Big). \end{aligned}$$

Applying Eq (5.20) to Eq (2.2), the multi-wave solution related to Eq (1.1) is obtained:

$$Q = \frac{N_Q(\rho)}{D_Q(\rho)}, \tag{5.21}$$

where

$$\begin{aligned} N_Q(\rho) =& \sqrt{2}\Big(l_1\sqrt{a_1 - a_2K - a_4K^2 - a_3V + \Theta}\, \sin\Big(d_4 - \tfrac{\sqrt{a_1-a_2K-a_4K^2-a_3V+\Theta}}{\sqrt{2}}\rho\Big) \\ &- l_0\sqrt{-a_1 + a_2K + a_4K^2 + a_3V - \Theta}\, \sinh\Big(d_2 - \tfrac{\sqrt{-a_1+a_2K+a_4K^2+a_3V-\Theta}}{\sqrt{2}}\rho\Big)\Big), \\ D_Q(\rho) =& l_1\cos\Big(d_4 - \tfrac{\sqrt{a_1-a_2K-a_4K^2-a_3V+\Theta}}{\sqrt{2}}\rho\Big) + l_2\cosh(d_6) + l_0\cosh\Big(d_2 - \tfrac{\sqrt{-a_1+a_2K+a_4K^2+a_3V-\Theta}}{\sqrt{2}}\rho\Big). \end{aligned}$$

These solutions represent the superposition of multiple wave modes, exhibiting coherent wave patterns with periodic and quasi-periodic characteristics under the chosen parameter regime. It should be noted that the multi-wave solution is well-defined provided that the denominators $D(\rho)$ and $D_Q(\rho)$ do not vanish. Therefore, the solution is valid in the domain where

$$D(\rho) \neq 0, \qquad D_Q(\rho) \neq 0.$$

For the parameter values considered in this work, these expressions remain strictly non-zero, ensuring that no singularity occurs in the presented wave profiles. Hence, the obtained multi-wave solution is regular and physically meaningful within the admissible parameter domain.

The obtained results highlight the diversity of nonlinear wave dynamics supported by the model. Breather solutions exhibit localized oscillatory behavior, M-shaped rational solutions demonstrate stable localized structures with a double-peak profile, while multi-wave solutions reveal coherent interactions among multiple wave components. Although some intermediate expressions in the solution process involve complex-valued quantities, the physically relevant wave solutions are obtained in real form by imposing suitable parameter constraints. In particular, complex conjugate pairs and appropriate choices of arbitrary constants ensure that the resulting wave fields are real-valued and physically meaningful.

6. Results and discussion

The dynamical system analysis provides qualitative information on wave behavior such as stability, periodicity, and possible chaotic transitions, while the Hirota bilinear method yields explicit analytical wave solutions. Both approaches are complementary, where the dynamical analysis describes the evolution properties of the system and the exact solutions represent its explicit wave structures under suitable parameter conditions.

This section provides a detailed description of the reported dynamical behaviors and analytical wave solutions for the eKP problem. Unlike a strictly descriptive approach, we emphasize the physical and mathematical significance of the findings, as well as their importance for previous research on KP-type models. Figure 1 illustrates the phase portraits of the unperturbed dynamical system (3.1) under two different parametric regimes: (a) $P > 0$ with parameters $\Theta = 1.1$, $a_4 = 1$, $a_3 = 1$, $a_2 = 1.2$, $a_1 = 0.2$, $V = 0.9$, $K = 2.5$; (b) $P < 0$ with parameters $\Theta = 1.1$, $a_4 = -1$, $a_3 = 1$, $a_2 = 1.2$, $a_1 = 0.2$, $V = 0.9$, $K = 2.5$. The acquired results show a qualitative change in system dynamics. For $P > 0$, the equilibrium point (A) functions as a center, providing closed trajectories corresponding to periodic wave motion, whereas point (B) acts as a saddle, producing separatrix structures. This shows the presence of both stable oscillatory waves and unstable wave transitions. For $P < 0$, the stability of equilibrium points is flipped, indicating that modest changes in system characteristics can greatly impact wave propagation behavior. Such bifurcation-induced transitions are consistent with previous research on KP-type systems, in which changes in parameters result in transitions between stable and unstable wave regimes. However, the inclusion of additional spatial coupling elements in the current model introduces richer dynamical patterns that are not observed in lower-dimensional KP equations.

Figures 2–5 present phase portraits and time series plots for the perturbed system (3.6) with parameters $P = 2$, $\delta = 0.5$, and $\mu = 0.6$ and different initial conditions such as $(0.6, 0.01)$, $(0.4, 0.01)$, $(0.9, 0.2)$, and $(0.2, 0.01)$. Unlike regular periodic motion, the trajectories create unusual attractors, and the time series show irregular, non-recurring oscillations. This confirms the existence of deterministic chaos. The major takeaway here is that chaotic wave structures form as a result of external disturbances and nonlinear interactions, which is extremely important in physical systems like nonlinear optics and plasma waves. Compared to prior literature, which frequently analyzes KP models for soliton solutions exclusively, this work broadens our understanding by demonstrating how chaotic regimes coexist with wave solutions, providing a fuller view of nonlinear wave evolution.

Figures 6 and 7 demonstrate multistability for parameters $P = 2$, $\delta = 0.5$, and $\mu = 0.6$ under specific conditions. In Figure 6(a) $(0.9, 0.2)$ (red curve), a chaotic orbit appears for $(0.9, 0.1)$ (blue curve). In Figure 6(b), periodic behavior is observed for the initial condition $(0.2, 0.01)$ (red curve), whereas chaotic behavior occurs for $(0.2, 0.3)$ (blue curve). In Figure 7(a), a periodic orbit appears for the initial condition $(0.9, 0.5)$ (red curve), while a chaotic orbit occurs for $(0.9, 0.4)$ (blue curve). In Figure 7(b), periodic behavior is observed for $(0.4, 0.01)$ (red curve), whereas chaotic behavior is obtained for $(0.4, 0.001)$ (blue curve). The results indicate that, depending on the initial conditions, the system can display several coexisting modes, including periodic, quasi-periodic, and chaotic behavior. This suggests the existence of numerous attractors in the same parameter regime. This phenomenon is especially significant since it emphasizes the non-uniqueness of wave evolution, which is rarely emphasized in traditional KP research. In contrast to previous studies that focused on single-solution dynamics, the current findings show that the same system may support many wave patterns at the same time, increasing its application in complicated physical contexts.

Figure 9 illustrates the return map, where scattered points indicate non-periodic behavior, confirming sensitive dependence on initial conditions. These results provide deeper insight into routes to chaos, which are essential for understanding instability mechanisms in nonlinear wave systems. Figures 11 and 12 show time series plots for slightly different initial conditions such as $(0.02, 0)$, $(0.03, 0)$, and $(0.04, 0)$. The results show that even small changes in initial conditions cause considerable variations in amplitude and waveform evolution. This illustrates the system's high sensitivity and nonlinearity, which is critical for practical applications requiring predictability.

Figure 13 shows the breather solution for parameters $b_1 = 0.9$, $q = 0.8$, $b_2 = 0.7$, $b_4 = 0.5$, $r_1 = 0.09$, $r_2 = 0.4$, $K = 0.2$, $q_1 = 0.7$, $b_6 = 0.3$, $Y = 2$, $Z = 9$, $V = 0.4$, and $\Theta = 0.8$. The plots exhibit oscillatory wave behavior with periodic characteristics. Depending on the parameter selection, partial localization can be observed; however, the solution predominantly displays periodic features rather than strongly localized breather-type dynamics. Physically, they resemble transitory patterns in a nonlinear optical medium. Compared to traditional KP breathers, the current solution reflects multidimensional coupling effects, resulting in more complex oscillatory behavior.

Figure 14 presents the M-shaped rational solution for parameters $c_1 = 0.8$, $c_2 = 0.02$, $c_3 = 0.06$, $c_5 = 0.6$, $K = 0.9$, $\Theta = 0.93$, $V = 0.8$, $Y = 2$, and $Z = 3$. The solution exhibits a characteristic double-peak (M-shaped) profile with a central dip, demonstrating strong localization and structural stability. These solutions have a double-peak structure, indicating good localization and stability. M-shaped waves, as opposed to breather solutions, are more resilient to parameter fluctuations. Such structures have been observed in nonlinear optical systems, but now they are expanded to a higher-dimensional KP framework. Figure 15 illustrates multi-wave solutions for parameters $l_0 = 0.24$, $l_1 = 0.4$, $l_2 = 0.3$, $a_1 = 7$, $a_2 = 0.8$, $a_3 = 0.5$, $a_4 = 0.88$, $K = 0.8$, $V = 0.6$, $\Theta = 0.76$, $d_2 = 3$, $d_4 = 0.2$, and $d_6 = 4.5$. It highlights the interaction of multiple wave components, illustrating coherent structures that propagate without distortion.

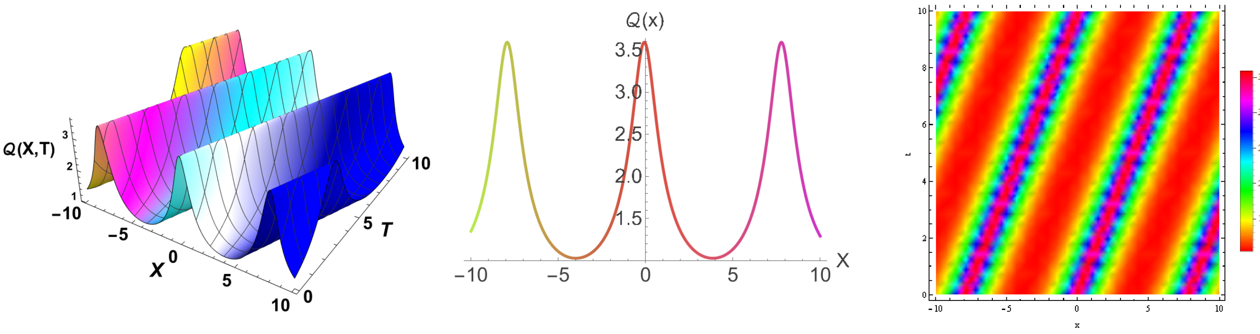

(a) 3D plot **(b)** 2D plot **(c)** contour plot

Figure 13. The 3D, 2D, and contour representations of the homoclinic breather solution given by Eq (5.11) for $b_1 = 0.9$, $q = 0.8$, $b_2 = 0.7$, $b_4 = 0.5$, $r_1 = 0.09$, $r_2 = 0.4$, $K = 0.2$, $q_1 = 0.7$, $b_6 = 0.3$, $Y = 2$, $Z = 9$, $V = 0.4$, $\Theta = 0.8$.

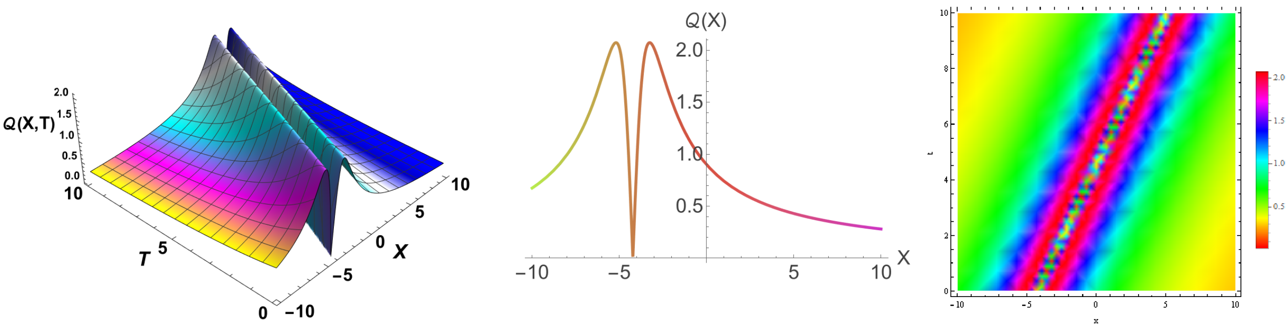

(a) 3D plot **(b)** 2D plot **(c)** contour plot

Figure 14. The 3D, 2D, and contour representations of the M-shaped rational solution presented in Eq (5.16) for $c_5 = 0.6$, $c_2 = 0.02$, $c_4 = 0.4$, $K = 0.9$, $\Theta = 0.93$, $Y = 2$, $Z = 3$, $V = 0.8$, $c_3 = 0.06$, $c_1 = 0.8$.

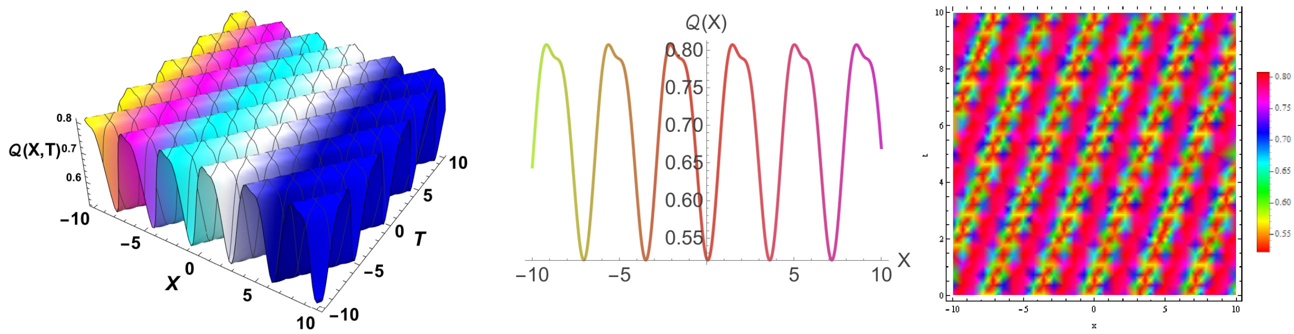

(a) 3D plot **(b)** 2D plot **(c)** contour plot

Figure 15. The 3D, 2D, and contour representations of the multi-wave solution derived by Eq (5.21) for $l_0 = 0.24$, $l_1 = 0.4$, $l_2 = 0.3$, $a_1 = 7$, $a_2 = 0.8$, $a_3 = 0.5$, $a_4 = 0.88$, $K = 0.8$, $V = 0.6$, $\Theta = 0.76$, $d_2 = 3$, $d_4 = 0.2$, $d_6 = 4.5$, $Y = 2$, $Z = 4$.

The graphical results show the coexistence of multiple wave modes forming structured periodic patterns. However, no strong nonlinear interaction between distinct localized solitons is observed for the present parameter set. The solution instead exhibits coherent multi-mode wave propagation with regular oscillatory behavior. The fundamental finding is that many waves can propagate simultaneously without losing their identity, demonstrating nonlinear superposition and coherent interaction. Such interactions are especially important in multimode optical fibers and plasma systems, extending past KP research by integrating multi-directional coupling and interaction dynamics.

7. Future direction and practical implementation

The findings of this study provide several promising directions for both future research and practical implementations in nonlinear science and applied physics. The comprehensive dynamical analysis of the eKP equation, including bifurcation behavior, chaotic dynamics, multistability, and sensitivity to initial conditions, offers deeper insight into the mechanisms governing complex nonlinear wave propagation. Such understanding is particularly valuable in nonlinear optical systems, where controlling wave stability and energy localization is crucial for improving signal transmission in optical fibers and multimode waveguides. The obtained breather, M-shaped rational, and multi-wave solutions reveal different types of localized structures and wave interactions that may contribute to the design of advanced optical communication technologies and the management of rogue-wave-like phenomena. Moreover, the analytical framework combining dynamical systems theory with Hirota's bilinear method provides a methodological foundation that can be extended to other high-dimensional nonlinear evolution equations. This may facilitate future investigations into wave dynamics in fluid mechanics, plasma physics, and complex dispersive media, where similar nonlinear interactions occur. In addition, the identification of chaotic regimes and sensitivity characteristics could guide the development of control strategies for nonlinear wave systems and inspire further studies on higher-order perturbations, numerical stabilization techniques, and wave interaction phenomena in multidimensional nonlinear models. These perspectives demonstrate that the present results not only enrich the theoretical understanding of soliton dynamics, but also open pathways for practical applications in modern nonlinear wave technologies.

8. Conclusions

This study presents a combined dynamical and analytical investigation of the eKP equation. The analysis integrates qualitative theory, bifurcation analysis, chaos detection techniques, sensitivity analysis, and the construction of exact solutions to provide insight into the nonlinear wave dynamics governed by this higher-dimensional model. By applying a traveling-wave transformation, the governing nonlinear partial differential equation is reduced to a planar dynamical system, enabling phase-plane analysis.

The bifurcation behavior of equilibrium points, illustrated through phase portraits, shows that for $P > 0$, closed trajectories correspond to periodic motions, while saddle points generate separatrix structures. For $P < 0$, the stability characteristics are altered, indicating that variations in system parameters can influence the qualitative behavior of wave propagation. The introduction of an external perturbation leads to more complex dynamics. The phase portraits and time series plots indicate irregular, aperiodic oscillations, suggesting the presence of chaotic behavior. In addition, multistability is observed, where different initial conditions give rise to coexisting periodic, quasi-periodic, and chaotic states. These findings highlight the sensitivity of the system to both parameters and initial conditions. Sensitivity analysis further demonstrates that small variations in initial conditions can produce noticeable changes in wave amplitude and evolution, reflecting the nonlinear and complex nature of the model. Such behavior may be relevant in applications where stability and predictability are important considerations. In addition to the dynamical analysis, several types of exact analytical solutions are derived using the bilinear method. The breather solutions represent localized oscillatory structures, the M-shaped rational solutions exhibit stable localized waveforms with a double-peak profile, and the multi-wave solutions describe interacting wave structures the multi-wave solutions describe the coexistence of multiple wave modes forming structured nonlinear wave patterns. These solution families illustrate the variety of wave patterns supported by the model and are broadly consistent with known behaviors in nonlinear wave systems.

Overall, the results provide a unified perspective on the interplay between dynamical behavior and exact solutions in the extended KP framework. While the findings extend existing studies by incorporating bifurcation and chaos analysis alongside analytical solutions, they remain within the broader context of KP-type models.

Future work may explore higher-order effects, additional perturbations, and numerical approaches to further investigate wave interactions and potential applications in nonlinear optics, plasma physics, and related fields.

Author contributions

Ejaz Hussain: Software, formal analysis, methodology, editing, writing–review; Nida Raees: Software, review, and validation. Ali. H. Tedjani: Investigation, formal analysis; Yakup Yildrim: Review and investigation; Yakup Yildirim: Formal analysis, methodology, review; Taha Radwan: Investigation, validation, resources, funding acquisition. All authors have read and agreed to publish the manuscript.

Use of Generative-AI tools declaration

The authors declare that they have not used artificial intelligence (AI) tools in the creation of this article.

Acknowledgments

The researchers would like to thank the Deanship of Graduate Studies and Scientific Research at Qassim University (www.qu.edu.sa) for financial support (QU-APC-2026).

Conflict of interest

The authors declare no conflicts of interest to report regarding the present study.

References

1. J. Weiss, M. Tabor, G. Carnevale, The Painlevé property for partial differential equations, *J. Math. Phys.*, **24** (1983), 522–526. https://doi.org/10.1063/1.525721
2. M. J. Ablowitz, P. A. Clarkson, *Solitons, nonlinear evolution equations and inverse scattering*, Cambridge University Press, 1991.
3. R. Hirota, *The direct method in soliton theory*, Cambridge University Press, 2004.
4. P. J. Olver, *Applications of Lie groups to differential equations*, 2 Eds., New York: Springer, 1993. https://doi.org/10.1007/978-1-4612-4350-2
5. R. F. Zhang, S. Bilige, Bilinear neural network method to obtain the exact analytical solutions of nonlinear partial differential equations and its application to p-gBKP equation, *Nonlinear Dyn.*, **95** (2019), 3041–3048. https://doi.org/10.1007/s11071-018-04739-z
6. J. Sirker, R. G. Pereira, I. Affleck, Conservation laws, integrability, and transport in one-dimensional quantum systems, *Phys. Rev. B*, **83** (2011), 035115. https://doi.org/10.1103/PhysRevB.83.035115
7. Y. Jiang, B. Tian, P. Wang, K. Sun, Infinitely-many conservation laws for two (2+1)-dimensional nonlinear evolution equations in fluids, *Pramana*, **83** (2014), 29–37. https://doi.org/10.1007/s12043-014-0763-0
8. W. X. Ma, W. Strampp, An explicit symmetry constraint for the Lax pairs and the adjoint Lax pairs of AKNS systems, *Phys. Lett. A*, **185** (1994), 277–286. https://doi.org/10.1016/0375-9601(94)90616-5
9. R. F. Zhang, M. C. Li, Bilinear residual network method for solving the exactly explicit solutions of nonlinear evolution equations, *Nonlinear Dyn.*, **108** (2022), 521–531. https://doi.org/10.1007/s11071-022-07207-x
10. Y. H. Yin, X. Lü, W. X. Ma, Bäcklund transformation, exact solutions and diverse interaction phenomena to a (3+1)-dimensional nonlinear evolution equation, *Nonlinear Dyn.*, **108** (2022), 4181–4194. https://doi.org/10.1007/s11071-021-06531-y
11. Y. Y. Xie, L. F. Li, Multiple-order breathers for a generalized (3+1)-dimensional Kadomtsev-Petviashvili Benjamin-Bona-Mahony equation near the offshore structure, *Math. Comput. Simul.*, **193** (2022), 19–31. https://doi.org/10.1016/j.matcom.2021.08.021
12. L. F. Li, Y. Y. Xie, Rogue wave solutions of the generalized (3+1)-dimensional Kadomtsev-Petviashvili equation, *Chaos Solitons Fract.*, **147** (2021), 110935. https://doi.org/10.1016/j.chaos.2021.110935
13. L. F. Li, Y. F. Nie, M. T. Zhu, Y. Y. Xie, Variable separation solution and multi-valued soliton of an extended (3+1)-dimensional B-type Kadomtsev-Petviashvili equation, *Nonlinear Dyn.*, **111** (2023), 4723–4736. https://doi.org/10.1007/s11071-022-08092-0
14. K. R. Raslan, T. S. EL-Danaf, K. K. Ali, Exact solution of the space-time fractional coupled EW and coupled MEW equations, *Eur. Phys. J. Plus*, **132** (2017), 319. https://doi.org/10.1140/epjp/i2017-11590-9

15. B. İnan, K. K. Ali, A. Saha, T. Ak, Analytical and numerical solutions of the Fitzhugh-Nagumo equation and their multistability behavior, *Numer. Methods Partial Differ. Equ.*, **37** (2021), 7–23. https://doi.org/10.1002/num.22516

16. A. M. Abdelwahab, K. S. Mekheimer, K. K. Ali, A. EL-Kholy, N. S. Sweed, Numerical simulation of electroosmotic force on micropolar pulsatile bloodstream through aneurysm and stenosis of carotid, *Waves Random Complex Media*, **34** (2024), 4288–4319. https://doi.org/10.1080/17455030.2021.1989517

17. K. K. Ali, S. B. G. Karakoç, H. Rezazadeh, Optical soliton solutions of the fractional perturbed nonlinear Schrödinger equation, *TWMS J. Appl. Eng. Math.*, **10** (2020), 930–939.

18. R. Seydel, *Practical bifurcation and stability analysis*, 3 Eds., New York: Springer, 2010. https://doi.org/10.1007/978-1-4419-1740-9

19. K. Nandakumar, J. H. Masliyah, Bifurcation in steady laminar flow through curved tubes, *J. Fluid Mech.*, **119** (1982), 475–490. https://doi.org/10.1017/S002211208200144X

20. R. K. Upadhyay, P. Roy, Spread of a disease and its effect on population dynamics in an ecoepidemiological system, *Commun. Nonlinear Sci. Numer. Simul.*, **19** (2014), 4170–4184. https://doi.org/10.1016/j.cnsns.2014.04.016

21. P. L. Li, R. Gao, C. J. Xu, J. W. Shen, S. Ahmad, Y. Li, Exploring the impact of delay on Hopf bifurcation of a type of BAM neural network models concerning three nonidentical delays, *Neural Process. Lett.*, **55** (2023), 11595–11635. https://doi.org/10.1007/s11063-023-11392-0

22. X. H. Zhu, P. F. Xia, Q. Z. He, Z. W. Ni, L. P. Ni, Coke price prediction approach based on dense GRU and opposition-based learning salp swarm algorithm, *Int. J. Bio Inspired Comput.*, **21** (2023), 106–121. https://doi.org/10.1504/IJBIC.2023.130549

23. M. M. Roshid, M. M. Rahman, Bifurcation analysis, modulation instability and optical soliton solutions and their wave propagation insights to the variable coefficient nonlinear Schrödinger equation with Kerr law nonlinearity, *Nonlinear Dyn.*, **112** (2024), 16355–16377. https://doi.org/10.1007/s11071-024-09872-6

24. A. Chakraborty, P. Veeresha, A. Ciancio, H. M. Baskonus, M. Alsulami, The effect of climate change on the dynamics of a modified surface energy balance-mass balance model of Cryosphere under the frame of a non-local operator, *Results Phys.*, **54** (2023), 107031. https://doi.org/10.1016/j.rinp.2023.107031

25. Y. L. Ma, A. M. Wazwaz, B. Q. Li, New extended Kadomtsev-Petviashvili equation: multiple soliton solutions, breather, lump and interaction solutions, *Nonlinear Dyn.*, **104** (2021), 1581–1594. https://doi.org/10.1007/s11071-021-06357-8

26. Y. L. Ma, A. M. Wazwaz, B. Q. Li, Novel bifurcation solitons for an extended Kadomtsev-Petviashvili equation in fluids, *Phys. Lett. A*, **413** (2021), 127585. https://doi.org/10.1016/j.physleta.2021.127585

27. N. H. Aljahdaly, H. A. Ashi, A. M. Wazwaz, S. A. El-Tantawy, Exponential time differencing scheme for modeling the dissipative Kawahara solitons in a two-electrons collisional plasma, *Rom. Rep. Phys.*, **74** (2022), 109.

28. A. M. Wazwaz, W. Alhejaili, S. A. El-Tantawy, New (3+1)-dimensional Painlevé integrable extensions of Mikhailov-Novikov-Wang equation: variety of multiple soliton solutions, *Rom. J. Phys.*, **67** (2022), 115.

29. J. G. Rao, B. A. Malomed, D. Mihalache, J. S. He, General higher-order breathers and rogue waves in the two-component long-wave–short-wave resonance interaction model, *Stud. Appl. Math.*, **149** (2022), 843–878. https://doi.org/10.1111/sapm.12523

30. J. G. Rao, D. Mihalache, J. S. He, F. Zhou, Degenerate and non-degenerate vector solitons and their interactions in the two-component long-wave–short-wave model of Newell type, *Chaos Solitons Fract.*, **166** (2023), 112963. https://doi.org/10.1016/j.chaos.2022.112963

31. A. M. Wazwaz, Variants of a (3+1)-dimensional generalized BKP equation: multiple-front waves solutions, *Comput. Fluids*, **97** (2014), 164–167. https://doi.org/10.1016/j.compfluid.2014.04.014

32. A. M. Wazwaz, Extensions of Kadomtsev-Petviashvili and Kadomtsev-Petviashvili-Boussinesq equations: multiple solitons and lump wave solutions, *Rom. Rep. Phys.*, **77** (2025), 115. https://doi.org/10.59277/RomRepPhys.2025.77.115

33. G. F. Han, X. Y. Li, Q. L. Zhao, C. Z. Li, Interaction structures of multi localized waves within the Kadomtsev-Petviashvili I equation, *Phys. D Nonlinear Phenom.*, **446** (2023), 133671. https://doi.org/10.1016/j.physd.2023.133671

34. G. F. Han, Y. Kodama, C. Z. Li, L. Sun, Regularizations for shock and rarefaction waves in the perturbed solitons of the KP equation, 2025, arXiv: 2503.01093.

35. C. Z. Li, Extensions on two-component BKP and D type Drinfeld-Sokolov hierarchies, *Anal. Math. Phys.*, **11** (2021), 83. https://doi.org/10.1007/s13324-021-00514-3

36. Z. Li, E. Hussain, Qualitative analysis and traveling wave solutions of a (3+1)-dimensional generalized nonlinear Konopelchenko-Dubrovsky-Kaup-Kupershmidt system, *Fractal Fract.*, **9** (2025), 285. https://doi.org/10.3390/fractalfract9050285

37. S. A. A. Shah, E. Hussain, W. X. Ma, Z. Li, A. E. Ragab, T. M. Khalaf, Qualitative analysis and new variety of soliton profiles for the (1+1)-dimensional modified equal width equation, *Chaos Solitons Fract.*, **187** (2024), 115353. https://doi.org/10.1016/j.chaos.2024.115353

38. Z. Li, J. J. Lyu, E. Hussain, Bifurcation, chaotic behaviors and solitary wave solutions for the fractional Twin-Core couplers with Kerr law non-linearity, *Sci. Rep.*, **14** (2024), 22616. https://doi.org/10.1038/s41598-024-74044-w

39. Beenish, M. Samreen, Bifurcation, multistability, and soliton dynamics in the stochastic potential Korteweg-de Vries equation, *Int. J. Theor. Phys.*, **64** (2025), 131. https://doi.org/10.1007/s10773-025-06000-x

40. A. Wolf, J. B. Swift, H. L. Swinney, J. A. Vastano, Determining Lyapunov exponents from a time series, *Phys. D Nonlinear Phenom.*, **16** (1985), 285–317. https://doi.org/10.1016/0167-2789(85)90011-9

41. E. Hussain, Z. Li, S. A. A. Shah, E. A. Az-Zo'bi, M. Hussien, Dynamics study of stability analysis, sensitivity insights and precise soliton solutions of the nonlinear (STO)-Burger equation, *Opt. Quantum Electron.*, **55** (2023), 1274. https://doi.org/10.1007/s11082-023-05588-w

42. E. Hussain, Y. Arafat, S. Malik, F. S. Alshammari, The (2+1)-dimensional chiral nonlinear Schrödinger equation: extraction of soliton solutions and sensitivity analysis, *Axioms*, **14** (2025), 422. https://doi.org/10.3390/axioms14060422

43. A. R. Seadawy, M. Younis, A. Althobaiti, Various forms of M-shaped rational, periodic cross kink waves and breathers for Bose-Einstein condensate model, *Opt. Quantum Electron.*, **54** (2022), 152. https://doi.org/10.1007/s11082-021-03498-3

44. L. Dieli, D. Pierangeli, F. Baronio, S. Trillo, C. Conti, Observation of lump solitons, *Phys. Rev. Lett.*, **136** (2026), 053804. https://doi.org/10.1103/ggbs-y21w

45. L. Liu, W. R. Sun, B. A. Malomed, Formation of rogue waves and modulational instability with zero-wavenumber gain in multicomponent systems with coherent coupling, *Phys. Rev. Lett.*, **131** (2023), 093801. https://doi.org/10.1103/PhysRevLett.131.093801

46. L. Liu, W. R. Sun, B. A. Malomed, P. G. Kevrekidis, Time-localized dark modes generated by zero-wave-number-gain modulational instability, *Phys. Rev. A*, **108** (2023), 033504. https://doi.org/10.1103/PhysRevA.108.033504

47. S. T. R. Rizvi, A. R. Seadawy, M. A. Ashraf, M. Younis, A. Khaliq, D. Baleanu, Rogue, multi-wave, homoclinic breather, M-shaped rational and periodic-kink solutions for a nonlinear model describing vibrations, *Results Phys.*, **29** (2021), 104654. https://doi.org/10.1016/j.rinp.2021.104654

48. S. A. M. Alsallami, S. T. R. Rizvi, A. R. Seadawy, Study of stochastic-fractional Drinfel'd-Sokolov-Wilson equation for M-shaped rational, homoclinic breather, periodic and kink-cross rational solutions, *Mathematics*, **11** (2023), 1504. https://doi.org/10.3390/math11061504

49. M. Z. Baber, S. Malik, M. W. Yasin, N. Ahmed, H. Rezazadeh, S. M. Ali, et al., Breathers, lump, M-shapes and other optical soliton interactions for the GRIN multimode optical fiber, *Int. J. Theor. Phys.*, **63** (2024), 245. https://doi.org/10.1007/s10773-024-05763-z

AIMS Press